Remarkable thermoelectric performance in BaPdS_{2} via pudding-mold band structure, band convergence, and ultralow lattice thermal conductivity

Eric B. Isaacs and Chris Wolverton

Phys. Rev. Materials **3**, 015403 — Published 28 January 2019

DOI: 10.1103/PhysRevMaterials.3.015403

Remarkable thermoelectric performance in $BaPdS_2$ via pudding-mold band structure, band convergence, and ultralow lattice thermal conductivity

Eric B. Isaacs and Chris Wolverton*
Department of Materials Science and Engineering, Northwestern University, Evanston, Illinois 60208, USA
(Dated: January 8, 2019)

Efficient thermoelectric materials require a rare and contraindicated combination of materials properties: large electrical conductivity, large Seebeck coefficient, and low thermal conductivity. One strategy to achieve the first two properties is via low-energy electronic bands containing both flat and dispersive parts in different regions of crystal momentum space, known as a pudding-mold band structure. Here, we illustrate that $BaPdS_2$ successfully achieves the pudding-mold band structure for the valence band, contributing to a large p-type thermoelectric power factor, due to its anisotropic crystal structure containing zig-zag chains of edge-sharing square planar PdS_4 units; large power factor is achieved for n-type doping as well due to band convergence. In addition, $BaPdS_2$ exhibits ultralow lattice thermal conductivity, and thus also achieves the third property, due to extremely soft and anharmonic interactions in its transverse acoustic phonon branch. We predict a remarkably large thermoelectric figure of merit, with peak values between 2 and 3 for two of the three crystallographic directions, suggesting $BaPdS_2$ warrants experimental investigation.

I. INTRODUCTION

The figure of merit for a thermoelectric material, which can convert a temperature gradient into electrical current, is

$$ZT = \frac{S^2\sigma}{\kappa_{el} + \kappa_L}T, \tag{1}$$

where S, σ, T, κ_{el}, and κ_L are the Seebeck coefficient, electrical conductivity, temperature, electrical contribution to thermal conductivity, and lattice contribution to thermal conductivity, respectively.[1,2] One strategy to achieve a large ZT is via engineering the electronic band structure, i.e., the electron energy ε as a function of crystal momentum $\mathbf{k}$.[3] In particular, a band with both flat (small $\nabla_{\mathbf{k}}\varepsilon$) and dispersive (large $\nabla_{\mathbf{k}}\varepsilon$) parts along a direction in $\mathbf{k}$-space has been shown to enhance σS^2 if the electron chemical potential μ lies at an energy separating the two regions.[4] In such a "pudding-mold" band structure, the band velocity difference leads to large S, and large σ is achieved due to the dispersive part of the band and a large Fermi surface.[4] More generally, one can consider a broader definition of a pudding-mold band structure in which the flat and dispersive regions can along different directions in $\mathbf{k}$-space, which naturally occurs for low-dimensional bulk and nanostructured crystals.[5–7] The pudding-mold band structure has been used to explain the promising thermoelectric performance of Na_xCoO_2,[4] SnSe,[8–10] and recently-proposed Fe-based Heusler compounds[11] among others.

Recently, the promising thermoelectric performance of several Pd oxide compounds has been attributed in part to the pudding-mold band structure. The layered compound $PbPdO_2$, for example, exhibits a large Seebeck coefficient of 175 μV/K at 600 K when hole doped.[12] Based on first-principles calculations, hole-doped Bi_2PdO_4 was predicted to exhibit high power factor (σS^2) in addition to low κ_L.[13] In both of these compounds, achieving the pudding-mold band structure appears to be connected to the presence of square planar Pd^{2+}. Based on this observation, we previously developed an inverse band structure design approach based on a materials database screening to search for other square planar compounds achieving the pudding-mold band structure.[14] Although several chemistries were considered, we focused on oxide materials such as Ba_2PdO_3 and La_4PdO_7 in order to validate the approach.

The thermoelectric efficiency of oxides is often limited by (1) large κ_L, stemming from the low atomic mass of oxygen and rigid chemical bonding, and (2) low carrier mobility.[15,16] Therefore, in this work, we turn our attention to *chalcogenide* materials. Chalcogenides comprise many of the most-investigated and highest-performance thermoelectrics, such as PbTe, Bi_2Te_3, SnSe, $Cu_2(S/Se)$, and $La_{3-x}Te_4$.[17–19] We investigate a chalcogenide material based on square planar Pd, namely $BaPdS_2$, with the aim of achieving low κ_L in addition to pudding-mold band structure. $BaPdS_2$ is the only such square planar chalcogenide identified by our previous inverse band structure design approach[14] other than metallic $EuPd_3S_4$[20] and the binaries PdS_2[21] and $PdSe_2$.[22] Although $BaPdS_2$ was first synthesized in 1986,[23] it has not been explored as a thermoelectric material to the best of our knowledge. The presence of heavy Ba, in addition to the lack of oxygen, leads to the potential for low κ_L. Using electronic structure and transport calculations based on the density functional theory, we find that $BaPdS_2$ exhibits (1) large p-type power factor stemming from a pudding-mold valence band structure, (2) large n-type power factor due to band convergence in the conduction band, (3) ultralow κ_L due to extremely soft and anharmonic bonding, and (4) highly-anisotropic electronic and thermal transport behavior. We find remarkable predicted thermoelectric performance, with ZT larger than 2 in certain crystallographic directions at high temperature, assuming optimal doping and using a rea-

sonable value of electronic relaxation time τ (5 fs).[11,24–28] Based on these results, we suggest $BaPdS_2$ warrants experimental investigation.

II. COMPUTATIONAL DETAILS

We perform density functional theory[29,30] calculations using the generalized gradient approximation[31] and the projector augmented wave method (Ba_sv, Pd, and S potentials)[32,33] in the Vienna *ab initio* simulation package (VASP).[34–37] A plane wave basis with 500 eV kinetic energy cutoff and uniform k-meshes with ≥ 700 k-points per $Å^{-3}$ are employed. The ionic forces and total energy are converged to 10^{-3} eV/Å and 10^{-6} eV, respectively. High-symmetry k- and q-point paths are based on the conventions of Setyawan *et al.*[38]

Semiclassical electronic transport calculations within the constant relaxation time (τ) approximation are performed using BOLTZTRAP[39] with k-point density of $3{,}500/Å^{-3}$. Although the use of an isotropic relaxation time is an approximation, previous studies suggest only minor anisotropy in τ even in highly anisotropic crystal structures.[39] Phonon calculations are performed using the direct approach in PHONOPY[40] with a 192-atom supercell chosen to be approximately cubic based on the algorithm of Erhart *et al.*[41] as implemented in ASE.[42] The mode Grüneisen parameter is computed using a $\pm 0.3\%$ volume difference. κ_L is computed via the Debye-Callaway model[43–45] and compared to that of the minimum thermal conductivity model of Cahill *et al.*[46] κ_{el} is computed via the Wiedemann-Franz law. Additional details on the electronic and thermal transport calculations are included in the Supplemental Material.[47]

III. RESULTS AND DISCUSSION

$BaPdS_2$, shown in Fig. 1(a) and Fig. 1(b), has a C-centered orthorhombic unit cell with space group $Cmcm$. Isostructural to $BaNiO_2$, it consists of 1D chains of edge-sharing PdS_4 square planar units (corresponding to a PdS_2 composition) connected in a zig-zag pattern. The computed lattice parameters, atomic positions, and formation energy are in excellent agreement with experimental values, as discussed in the Supplemental Material. The electronic band structure of $BaPdS_2$ is shown in Fig. 1(c). The valence band, which consists primarily of Pd d states, exhibits a pudding-mold band structure. It is dispersive in the direction along the 1D chains (e.g., Γ–Z) and flat along other directions (e.g., Γ–X and Γ–Y). In order words, the pudding-mold band structure is closely related to the highly-anisotropic crystal structure of $BaPdS_2$. We do not find a pudding-mold band structure for the conduction band, which consists of a hybridization of Pd d and S p orbitals. We note that an additional conduction band minimum between S and R is close in energy (∼130 meV) to the band edge at Γ.

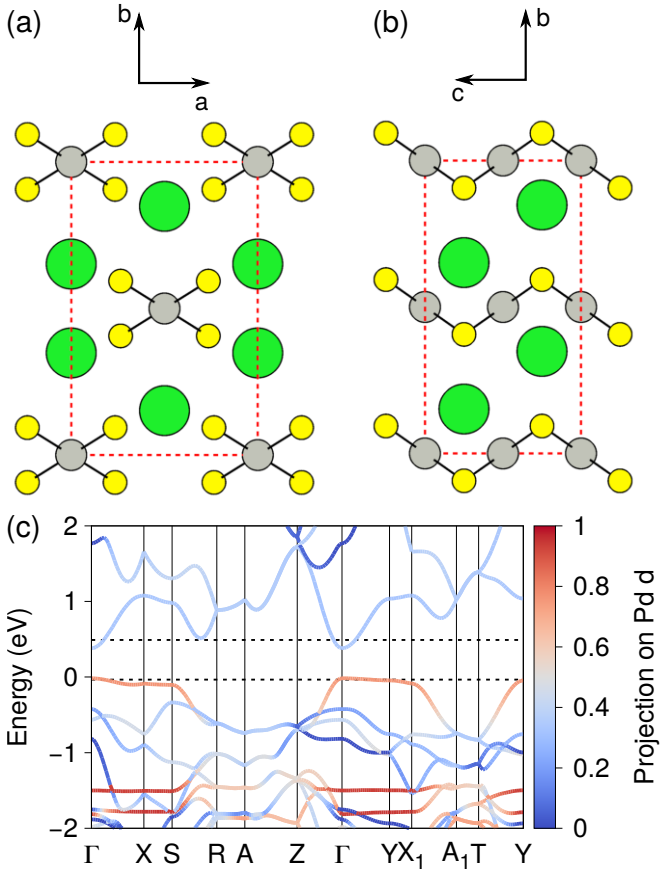

FIG. 1. Orthographic projection of the crystal structure of $BaPdS_2$ along the (a) **c** and (b) **a** axes of the conventional unit cell (red dashed lines). The green, gray, and yellow circles represent Ba, Pd, and S atoms, respectively. Black lines indicate the Pd–S bonds of the square planar units. (c) The electronic bands of $BaPdS_2$ colored by the Pd d character of the electronic states. The zero of energy is set to the valence band maximum, and the black horizontal dotted lines indicate the $\pm 10^{20}$ cm^{-3} doping levels.

The band structure of $BaPdS_2$ leads to notable electronic transport properties. Figure 2(a) illustrates the behavior of the average (over Cartesian directions) of $\sigma S^2/\tau$ as a function of carrier concentration for several temperatures. Results for $BaPdS_2$ are shown in comparison to those of SnSe, a high-performing thermoelectric material.[8,48–50] $BaPdS_2$ achieves comparable p-type power factor behavior to SnSe, albeit at larger (though still reasonable[17]) doping values. For example, at 700 K, the maximum predicted p-type $\sigma S^2/\tau$ is $\sim 3 \times 10^{11}$ W/(m·K²·s) for both $BaPdS_2$ (for 7×10^{20} holes/cm³) and SnSe (for 3×10^{20} holes/cm³). We also note that the p-type power factor behavior exhibits significantly less temperature dependence for $BaPdS_2$ than for SnSe. Although the conduction band does not exhibit pudding-mold qualities, we find even larger $\sigma S^2/\tau$ for n-type doping, though smaller than the corresponding SnSe behavior. For example, the peak n-type $\sigma S^2/\tau$

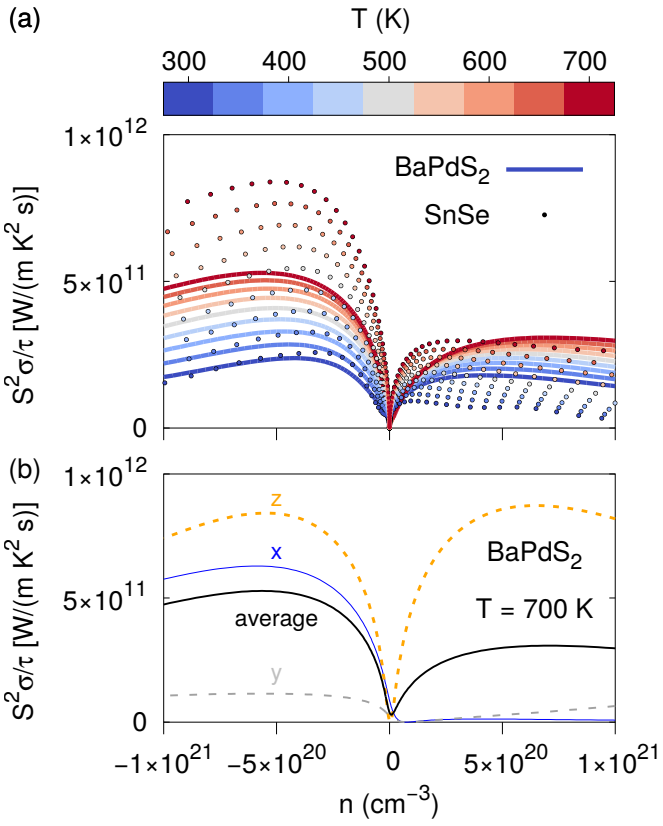

FIG. 2. (a) Power factor divided by electronic relaxation time as a function of carrier concentration for $BaPdS_2$ (lines) and SnSe (circles), averaged over the x, y, and z directions, for several values of T. (b) $T = 700$ K power factor divided by electronic relaxation time versus carrier concentration in each direction, in addition to the average, for $BaPdS_2$.

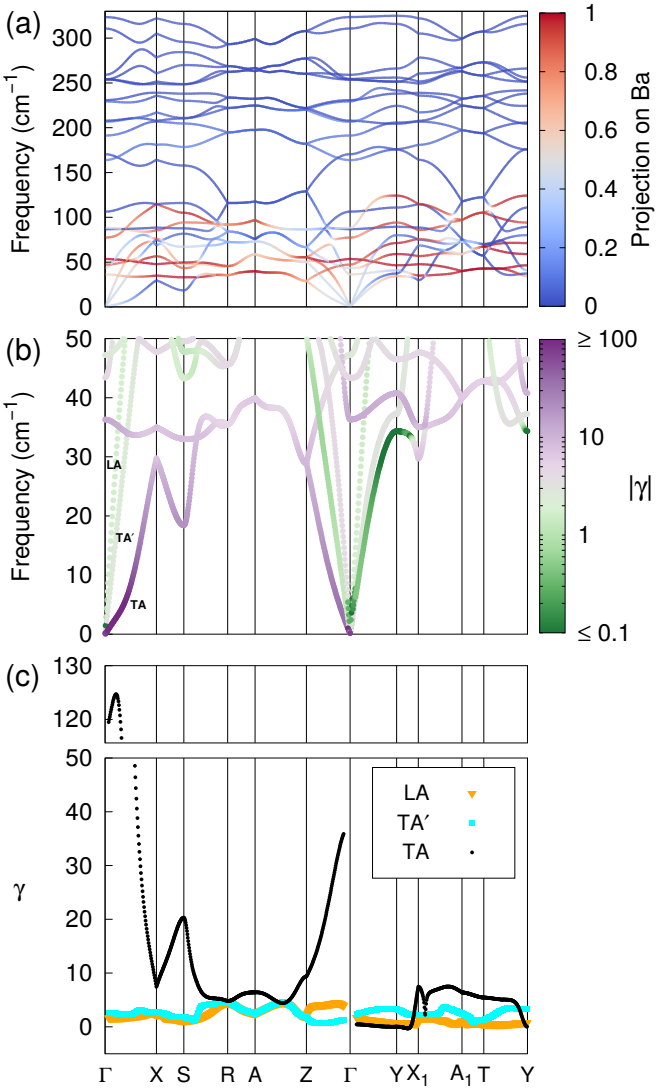

FIG. 3. (a) $BaPdS_2$ phonon bands colored by Ba contribution to the phonon eigenvector. (b) The low-frequency portion of the phonon dispersion with bands colored by the magnitude of the mode Grüneisen parameter. (c) Dispersion of the mode Grüneisen parameter $\gamma_{\mathbf{q}\nu}$ for the acoustic branches. Due to the large $\gamma_{\mathbf{q}\nu}$ values for the TA branch along Γ–X, we use a broken $\gamma_{\mathbf{q}\nu}$ axis for clarity.

for $BaPdS_2$ at 700 K is 5.3×10^{11} W/(m·K^2·s), occurring at a doping value of $\sim 5.5 \times 10^{20}$ electrons/cm^3; SnSe exhibits a significantly larger peak n-type $\sigma S^2/\tau$ of 8.4×10^{11} W/(m·K^2·s) at around the same doping magnitude. The appreciable n-type power factor behavior for $BaPdS_2$ likely stems from the band convergence,[51–55] i.e., the small energy separation between the conduction band minima (1) at Γ and (2) between S and R. Although the conduction band minimum at Γ is singly degenerate, the band minimum between S and R has a higher degeneracy of 4, contributing to a large Seebeck coefficient.

Due to the structural anisotropy, the power factor behavior for $BaPdS_2$ is highly anisotropic. We illustrate the power factor behavior at 700 K, for example, in Fig. 2(b) for each direction. For hole doping, $\sigma S^2/\tau$ is only appreciable along the z direction (i.e., along the 1D chains), which is consistent with the pudding-mold band structure. In contrast, for electron doping, large $\sigma S^2/\tau$ is observed in both the z and x directions. A rationalization for the lower n-type power factor behavior in the y direction is discussed in the Supporting Information.

Having established the promising predicted electronic

Branch	v_x	v_y	v_z	$\Theta_{\Gamma X}$	$\Theta_{\Gamma Y}$	$\Theta_{\Gamma Z}$
TA	0.5	1.9	0.8	43	49	42
TA′	2.4	2.4	1.9	82	54	72
LA	4.1	3.7	3.6	99	115	72

TABLE I. Group velocity v at Γ (in km/s) and Debye temperature Θ (in K) of $BaPdS_2$ for each acoustic branch and direction.

transport properties of $BaPdS_2$, we now turn our attention to thermal transport. The phonon dispersion of $BaPdS_2$ is shown in Fig. 3(a). Low-frequency optical modes, primarily involving vibration of the heavy Ba atoms, are observed in the $\sim$ 30–110 cm^{-1} frequency range. For each acoustic branch, we compute the group velocity in the long-wavelength limit (v_x, v_y, and v_z) and Debye temperature ($\Theta_{\Gamma X}$, $\Theta_{\Gamma Y}$, and $\Theta_{\Gamma Z}$) for each direction, as shown in Table I. Here, we define Θ as the acoustic phonon frequency at the zone boundary, and the acoustic branch definitions are given in the Supplemental Material. $BaPdS_2$ is a very soft material, exhibiting low group velocities (0.5–4.1 km/s) and Debye temperatures (42–115 K). For comparison, v of 1.0–2.9 and Θ of 19–72 are found in SnSe.[8] The transverse acoustic (TA) branch of $BaPdS_2$ is particular soft, with $v = 0.5$ km/s (0.8 km/s) and $\Theta = 43$ K (42 K) along the x (z) direction. Animations of the TA phonons along X (featuring rigid PdS_2 chains sliding in the z direction with respect to the others) and along Z (featuring oscillations of the individual PdS_2 chains in the x direction) are included in the Supplemental Material. We note that the behavior of the TA branch is significantly harder along the y direction in terms of the group velocity (1.9 km/s), though not the Debye temperature (49 K). Corresponding to PdS_2 chains sliding in the z direction, the TA branch along Y corresponds to a similar atomic motion to that along X; the significantly larger inter-chain distance in the y direction (10.8 Å) compared to that in x direction (6.9 Å) may be responsible for the very different phonon properties.

	$BaPdS_2$				SnSe		
Branch	γ_{all}	$\gamma_{\Gamma X}$	$\gamma_{\Gamma Y}$	$\gamma_{\Gamma Z}$	$\gamma_{\Gamma X}$	$\gamma_{\Gamma Y}$	$\gamma_{\Gamma Z}$
TA	25.5	80.3	0.3	22.8	5.1	2.7	1.0
TA′	2.8	2.6	3.1	1.0	1.1	2.4	2.7
LA	2.3	2.1	1.2	4.0	5.9	1.3	3.3
Avg.	10.2	28.3	1.5	9.3	4.1	2.1	2.3

TABLE II. Averages (computed as $\sqrt{\langle\gamma^2\rangle}$) of mode Grüneisen parameter $\gamma_{\mathbf{q}\nu}$ for $BaPdS_2$ and SnSe[8] for different acoustic branches and directions. For $BaPdS_2$, the average over the entire high-symmetry path in the Brillouin zone is also given as γ_{all}.

To acquire a baseline assessment for the overall magnitude of the anharmonicity, i.e., the phonon-phonon scattering strength, we compute the mode Grüneisen parameter

$$\gamma_{\mathbf{q}\nu} = -\frac{\partial\omega_{\mathbf{q}\nu}/\omega_{\mathbf{q}\nu}}{\partial V/V}, \tag{2}$$

where V is the volume and $\omega_{\mathbf{q}\nu}$ is the phonon frequency for crystal momentum $\mathbf{q}$ and branch ν. The low-frequency phonons of $BaPdS_2$, colored by $|\gamma|$, are shown in Fig. 3(b), whereas the full dispersion of $\gamma_{\mathbf{q}\nu}$ for the acoustic branches is included in Fig. 3(c). The most prominent feature is that $BaPdS_2$ has gigantic $\gamma_{\mathbf{q}\nu}$ for the TA branch along Γ–X (values up to $\sim$ 125) and Γ–Z (values up to $\sim$ 35), which indicates extremely anharmonic interactions for this acoustic branch in $BaPdS_2$. We perform tests to confirm the large computed $\gamma_{\mathbf{q}\nu}$ are not a numerical artifact, as discussed in the Supplemental Material. Averages of the mode Grüneisen parameter for each acoustic branch of $BaPdS_2$, averaged over Γ–X, Γ–Y, Γ–Z, and the full high-symmetry path in the Brillouin zone, are shown in Table II, in which we also compare to literature results for SnSe.[8] The average $\gamma_{\mathbf{q}\nu}$ for the TA branch of $BaPdS_2$ is 80.3 in the x direction and 22.8 in the z direction, compared to much smaller (less anharmonic) values of 5.1 and 1.0 for SnSe in the corresponding directions. We note that a key exception to the large anharmonicity of the TA branch of $BaPdS_2$ is along the y direction, for which the average $\gamma_{\mathbf{q}\nu}$ is only 0.3, as compared to 2.7 for SnSe. In other words, the TA branch of $BaPdS_2$ is not only harder in the y direction than the other directions, but also much less anharmonic. Although the most remarkable finding is the extremely large $\gamma_{\mathbf{q}\nu}$ for the TA branch, we also find significant anharmonicity for other phonon branches. For example, the TA′ (LA) branch exhibits appreciable $\gamma_{\mathbf{q}\nu}$ of 1.0–3.1 (1.2–4.0), as compared to 1.1–2.7 (1.3–5.9) for SnSe. Large anharmonicity is also found in the lowest-frequency optical branch, with mode Grüneisen parameter values as large as $\sim$ 12, as shown in Fig. 3(b). This branch corresponds to oscillation of the Ba sublattice with respect to the PdS_2 chains in the z direction.

We employ the Debye-Callaway model, an approximate model taking into account normal and Umklapp acoustic phonon-phonon scattering via the mode Grüneisen parameter, as a means to estimate the lattice thermal conductivity of $BaPdS_2$.[43–45] We note that the low-frequency optical phonons with large $\gamma_{\mathbf{q}\nu}$, not taken into account in the Debye-Callaway model, may further lower κ_L compared to the values reported here. The contributions of each acoustic phonon branch to κ_L as a function of T in the x, y, and z directions are shown in Fig. 4(a)–4(c), respectively. $BaPdS_2$ exhibits ultralow lattice thermal conductivity (κ_L less than 1 W/m·K) in the x and z directions. In these directions, the predicted κ_L are of the same magnitude as that of SnSe along its smallest-κ_L direction (values of $\sim$ 0.25–0.7 W/m·K).[8] For $BaPdS_2$, the main contributor to κ_L in the x direction is the LA branch, which exhibits the largest group velocity; the main contributor in the z direction is the TA′ branch, which is the least anharmonic. Like the power factor, the thermal transport is highly anisotropic: in the y direction, κ_L is much larger (values of 4–8 W/m·K) than in the other directions, stemming primarily from the small $\gamma_{\Gamma Y}$ of 0.3 for the TA branch, as discussed above. In the x and z (but not y) directions, $BaPdS_2$ achieves the minimum possible κ_L, shown as red lines in Fig. 4(a)–4(c), estimated from the model of Cahill *et al.* Overall, $BaPdS_2$ is predicted to exhibit remarkably poor thermal transport in directions other than y.

As illustrated in Fig. 4(d)–4(f), the combination of

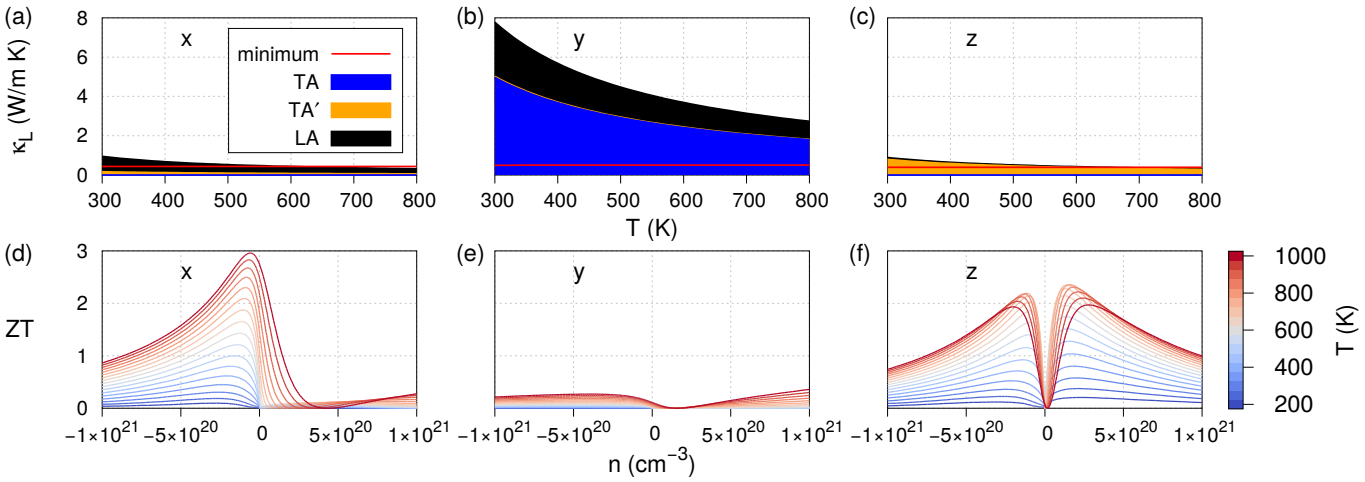

FIG. 4. (a)–(c) Stacked plots of $BaPdS_2$ acoustic branch contributions to κ_L versus T computed via the Debye-Callaway model for the (a) x, (b) y, and (c) z directions, respectively. Red lines indicate the minimum κ_L of the Cahill model. (d)–(f) ZT as a function of carrier concentration for different T in the (d) x, (e) y, and (f) z directions, respectively. Values are shown for $\tau = 5$ fs.

large power factor and low κ_L leads to impressive figure of merit for $BaPdS_2$, particularly in the x direction for electron doping and in the z direction for both electron and hole doping. At high temperature, we find peak ZT values of nearly 3 in the x direction (for 6.0×10^{19} electrons/cm^3) and values of nearly 2.3 in the z direction (for 1.1×10^{20} electrons/cm^3 or 1.6×10^{20} holes/cm^3). In contrast, much smaller peak ZT (< 1) is observed for $BaPdS_2$ in the y direction, due to the smaller power factor and larger κ_L. In order to obtain the predicted ZT values discussed above, we have chosen an electronic relaxation time (τ) of 5 fs. While an *ab initio* estimation of τ (e.g., from electron-phonon scattering calculations) will be important future work, we note that 5 fs is reasonable in terms of the order of magnitude[56,57] and can be considered a conservative estimate based on previous works.[11,24–28] Even with a less optimistic guess for the electronic scattering time, we still find quite large values for the thermoelectric figure of merit, albeit at larger doping. For example, assuming $\tau = 1$ fs, a peak ZT of 1.3 is achieved in the x direction for 2.0×10^{20} electrons/cm^3. Therefore, even with the uncertainty in τ, our results strongly suggest $BaPdS_2$ merits experimental investigation.

IV. CONCLUSIONS

$BaPdS_2$, previously identified by our inverse band structure design approach, is a square planar sulfide material with remarkable, anisotropic thermoelectric properties. Due to a pudding-mold valence band structure and multiple conduction bands, $BaPdS_2$ exhibits impressive power factor behavior in two of the crystallographic directions. With heavy Ba atoms and extremely soft and anharmonic bonding, $BaPdS_2$ achieves ultralow lattice thermal conductivity in the x and z directions. We predict peak ZT values of 2–3 in the x direction (n-type) and the z direction (n- and p-type) for an electronic relaxation time of 5 fs. Our results strongly suggest $BaPdS_2$ warrants experimental investigation for its remarkable electronic, thermal transport, and thermoelectric properties.

ACKNOWLEDGMENTS

We acknowledge support from the U.S. Department of Energy under Contract DE-SC0014520. Computational resources were provided by the National Energy Research Scientific Computing Center (U.S. Department of Energy Contract DE-AC02-05CH11231) and the Extreme Science and Engineering Discovery Environment (National Science Foundation Contract ACI-1548562).

* c-wolverton@northwestern.edu

[1] H. J. Goldsmid, *Introduction to Thermoelectricity*, Springer Series in Materials Science, Vol. 121 (Springer,

Berlin, Heidelberg, 2010).
[2] A. Zevalkink, D. M. Smiadak, J. L. Blackburn, A. J. Ferguson, M. L. Chabinyc, O. Delaire, J. Wang, K. Kovnir, J. Martin, L. T. Schelhas, T. D. Sparks, S. D. Kang, M. T. Dylla, G. J. Snyder, B. R. Ortiz, and E. S. Toberer, Appl. Phys. Rev. **5**, 021303 (2018).
[3] Y. Pei, H. Wang, and G. J. Snyder, Adv. Mater. **24**, 6125 (2012).
[4] K. Kuroki and R. Arita, J. Phys. Soc. Jpn. **76**, 083707 (2007).
[5] L. D. Hicks and M. S. Dresselhaus, Phys. Rev. B **47**, 12727 (1993).
[6] L. D. Hicks and M. S. Dresselhaus, Phys. Rev. B **47**, 16631 (1993).
[7] H. Usui and K. Kuroki, J. Appl. Phys. **121**, 165101 (2017).
[8] L.-D. Zhao, S.-H. Lo, Y. Zhang, H. Sun, G. Tan, C. Uher, C. Wolverton, V. P. Dravid, and M. G. Kanatzidis, Nature **508**, 373 (2014).
[9] K. Kutorasinski, B. Wiendlocha, S. Kaprzyk, and J. Tobola, Phys. Rev. B **91**, 205201 (2015).
[10] Z. Wang, C. Fan, Z. Shen, C. Hua, Q. Hu, F. Sheng, Y. Lu, H. Fang, Z. Qiu, J. Lu, Z. Liu, W. Liu, Y. Huang, Z.-A. Xu, D. W. Shen, and Y. Zheng, Nat. Commun. **9**, 47 (2018).
[11] D. I. Bilc, G. Hautier, D. Waroquiers, G.-M. Rignanese, and P. Ghosez, Phys. Rev. Lett. **114**, 136601 (2015).
[12] L. K. Lamontagne, G. Laurita, M. W. Gaultois, M. Knight, L. Ghadbeigi, T. D. Sparks, M. E. Gruner, R. Pentcheva, C. M. Brown, and R. Seshadri, Chem. Mater. **28**, 3367 (2016).
[13] J. He, S. Hao, Y. Xia, S. S. Naghavi, V. Ozoliņš, and C. Wolverton, Chem. Mater. **29**, 2529 (2017).
[14] E. B. Isaacs and C. Wolverton, Chem. Mater. **30**, 1540 (2018).
[15] J. He, Y. Liu, and R. Funahashi, J. Mater. Res. **26**, 1762 (2011).
[16] K. F. Garrity, Phys. Rev. B **94**, 045122 (2016).
[17] G. J. Snyder and E. S. Toberer, Nat. Mater. **7**, 105 (2008).
[18] X. Zhang and L.-D. Zhao, J. Materiomics **1**, 92 (2015).
[19] G. Tan, L.-D. Zhao, and M. G. Kanatzidis, Chem. Rev. **116**, 12123 (2016).
[20] K. L. Yao, L. Q. Wang, and Z. L. Liu, Solid State Comm. **130**, 741 (2004).
[21] R. Bhatt, S. Bhattacharya, R. Basu, A. Singh, U. Deshpande, C. Surger, S. Basu, D. K. Aswal, and S. K. Gupta, Thin Solid Films **539**, 41 (2013).
[22] J. Sun, H. Shi, T. Siegrist, and D. J. Singh, Appl. Phys. Lett. **107**, 153902 (2015).
[23] J. Huster and W. Bronger, J. Less Common Met. **119**, 159 (1986).
[24] G. K. H. Madsen, J. Am. Chem. Soc. **128**, 12140 (2006).
[25] A. N. Gandi and U. Schwingenschlögl, Chem. Mater. **26**, 6628 (2014).
[26] F. Q. Wang, S. Zhang, J. Yu, and Q. Wang, Nanoscale **7**, 15962 (2015).
[27] S. Hao, F. Shi, V. P. Dravid, M. G. Kanatzidis, and C. Wolverton, Chem. Mater. **28**, 3218 (2016).
[28] K. Pal, J. He, and C. Wolverton, Chem. Mater. **30**, 7760 (2018).
[29] P. Hohenberg and W. Kohn, Phys. Rev. **136**, B864 (1964).
[30] W. Kohn and L. J. Sham, Phys. Rev. **140**, A1133 (1965).
[31] J. P. Perdew, K. Burke, and M. Ernzerhof, Phys. Rev. Lett. **77**, 3865 (1996).
[32] P. E. Blöchl, Phys. Rev. B **50**, 17953 (1994).
[33] G. Kresse and D. Joubert, Phys. Rev. B **59**, 1758 (1999).
[34] G. Kresse and J. Hafner, Phys. Rev. B **49**, 14251 (1994).
[35] G. Kresse and J. Hafner, Phys. Rev. B **47**, 558 (1993).
[36] G. Kresse and J. Furthmüller, Phys. Rev. B **54**, 11169 (1996).
[37] G. Kresse and J. Furthmüller, Comput. Mater. Sci. **6**, 15 (1996).
[38] W. Setyawan and S. Curtarolo, Comput. Mater. Sci. **49**, 299 (2010).
[39] G. K. H. Madsen and D. J. Singh, Comput. Phys. Commun. **175**, 67 (2006).
[40] A. Togo, F. Oba, and I. Tanaka, Phys. Rev. B **78**, 134106 (2008).
[41] P. Erhart, B. Sadigh, A. Schleife, and D. Åberg, Phys. Rev. B **91**, 165206 (2015).
[42] A. H. Larsen, J. J. Mortensen, J. Blomqvist, I. E. Castelli, R. Christensen, M. Dułak, J. Friis, M. N. Groves, B. Hammer, C. Hargus, E. D. Hermes, P. C. Jennings, P. B. Jensen, J. Kermode, J. R. Kitchin, E. L. Kolsbjerg, J. Kubal, K. Kaasbjerg, S. Lysgaard, J. B. Maronsson, T. Maxson, T. Olsen, L. Pastewka, A. Peterson, C. Rostgaard, J. Schiøtz, O. Schütt, M. Strange, K. S. Thygesen, T. Vegge, L. Vilhelmsen, M. Walter, Z. Zeng, and K. W. Jacobsen, J. Phys. Condens. Matter **29**, 273002 (2017).
[43] J. Callaway, Phys. Rev. **113**, 1046 (1959).
[44] D. T. Morelli, J. P. Heremans, and G. A. Slack, Phys. Rev. B **66**, 195304 (2002).
[45] Y. Zhang, J. Materiomics **2**, 237 (2016).
[46] D. G. Cahill, S. K. Watson, and R. O. Pohl, Phys. Rev. B **46**, 6131 (1992).
[47] See Supplemental Material for additional details on electronic and thermal transport methods, phonon and anharmonicity calculation convergence, animations of several low-frequency phonon modes, comparison to experimental crystal structure and formation energy, and the electronic band structure for a different high-symmetry crystal momentum path.
[48] L.-D. Zhao, G. Tan, S. Hao, J. He, Y. Pei, H. Chi, H. Wang, S. Gong, H. Xu, V. P. Dravid, C. Uher, G. J. Snyder, C. Wolverton, and M. G. Kanatzidis, Science **351**, 141 (2015).
[49] A. T. Duong, V. Q. Nguyen, G. Duvjir, V. T. Duong, S. Kwon, J. Y. Song, J. K. Lee, J. E. Lee, S. Park, T. Min, J. Lee, J. Kim, and S. Cho, Nat. Commun. **7**, 13713 (2016).
[50] C. Chang, M. Wu, D. He, Y. Pei, C.-F. Wu, X. Wu, H. Yu, F. Zhu, K. Wang, Y. Chen, L. Huang, J.-F. Li, J. He, and L.-D. Zhao, Science **360**, 778 (2018).
[51] Y. Pei, X. Shi, A. LaLonde, H. Wang, L. Chen, and G. J. Snyder, Nature **473**, 66 (2011).
[52] W. Liu, X. Tan, K. Yin, H. Liu, X. Tang, J. Shi, Q. Zhang, and C. Uher, Phys. Rev. Lett. **108**, 166601 (2012).
[53] Y. Tang, Z. M. Gibbs, L. A. Agapito, G. Li, H.-S. Kim, M. B. Nardelli, S. Curtarolo, and G. J. Snyder, Nat. Mater. **14**, 1223 (2015).
[54] W. G. Zeier, A. Zevalkink, Z. M. Gibbs, G. Hautier, M. G. Kanatzidis, and G. J. Snyder, Angew. Chem. Int. Ed. **55**, 6826 (2016).
[55] W. G. Zeier, Curr. Opin. Green Sustain. Chem. **4**, 23 (2017).
[56] N. W. Ashcroft and N. D. Mermin, *Solid State Physics* (Saunders College Publishing, 1976).
[57] P. Y. Yu and M. Cardona, *Fundamentals of Semiconductors: Physics and Material Properties* (Springer-Verlag, 1996).